INTERNATIONAL JOURNAL OF AUTOMOTIVE AND MECHANICAL ENGINEERING
ISSN: 2229-8649 e-ISSN: 2180-1606
VOLUME 22, ISSUE 4, 2025, 13117 - 13130
DOI: https://doi.org/10.15282/ijame.22.4.2025.21.0998

RESEARCH ARTICLE

Optimal Configuration of a Rear Wing to Improve Stability and Aerodynamic Efficiency of a Sedan Using Computational Fluid Dynamics

Juan A. Guevara[1], Christian V. Rodriguez[1]*, Dennys D. De La Torre[2]

[1]Universidad Tecnológica del Perú, 15046 Lima, Perú
[2]Multidisciplinary Transport Research Group, Universidad Nacional de Ingeniería, Av. Túpac Amaru 210, Lima, Perú

ABSTRACT – The rear wing mounted on a sedan's trunk is primarily designed to enhance the car's aerodynamics, particularly when driving at high speeds. This component generates a downward force, which increases ground adhesion, improving stability during driving. This study aims to determine the optimal configuration of a rear wing installed on the trunk of a sedan to improve its stability and aerodynamic efficiency. Using the mesh selected from the independence study, through Computational Fluid Dynamics (CFD) method, we compared the lift (Cl) and drag (Cd) coefficients, as well as the lift to drag ratio (Cl/Cd) for different rear wings shaped by NACA 4412, SD7032, E387, NASA SC(2)-0714, and S826 profiles to find their optimal configuration. The simulations include angles of attack (α) between 0 and 15° and vehicle speeds of 36, 72, 108, and 144 km/h. Subsequently, we studied the fluid behavior around the sedan with and without the rear wing. Then, the rear wing height ratios (b/H) that show the best aerodynamic performance were analyzed. Apart from the NACA 4412 profile, the profiles used here have not been previously analyzed in rear-wing applications on sedans, which adds to the value of this research. The results show that, at various driving speeds of the sedan, different rear wings achieve the best Cl. The suitable configurations are NACA 4412 at α = 9° (for 36 km/h speed), S826 at α = 7° (for 72 and 108 km/h), and NASA SC(2)-0714 at α = 10° (for 144 km/h).

ARTICLE HISTORY
Received : 10th Feb. 2025
Revised : 10th Jul. 2025
Accepted : 30th Jul. 2025
Published : 21st Dec. 2025

KEYWORDS
Rear wing
Sedan car
Aerodynamic efficiency
CFD
Negative lift

1. INTRODUCTION

Vehicle manufacturers persistently research innovative methods to increase car efficiency [1]. These options are not limited to energy efficiency but also include integrating technologies to improve the vehicle's stability and maneuverability, especially during high-speed driving [2]. At high speeds, vehicle stability and maneuverability improve through modifications to aerodynamic forces, including lift (Fl) and drag (F_d) [3]. It's worth noting that a pressure differential generates lift, primarily due to the pressure difference between the object's top and bottom surfaces [4]. Notably, the air flowing around the vehicle separates at the rear, creating a large, turbulent, low-pressure region known as the wake, contributing to increased drag. Drag is unfavourable for vehicle movement as it opposes forward motion [5]. Therefore, appropriate vehicle design significantly influences drag reduction. According to [6], a car's F_d is determined by its geometry and surface. Therefore, researchers optimise vehicle shape to reduce its F_d [1]. The vehicle's shape affects fuel consumption, potentially saving about 3% in fuel during urban driving and 11% on highways by reducing F_d [7]. Accessories like rear wings and diffusers improve aerodynamic performance by enhancing downforce and road grip [4].

Aerodynamic car improvements can be achieved through experimentation or simulation using Computational Fluid Dynamics (CFD), relying on mass, momentum, and energy conservation principles. CFD allows us to simulate airflow patterns interacting with vehicle surfaces, predicting the aerodynamic forces generated [1]. Highway testing requires significant time and cost due to the numerous variables to investigate [4, 8]. In contrast, CFD dramatically reduces the time and expense of physical testing and prototyping [7]. Additionally, it is noteworthy that CFD results were only 2.68% different from experimental validation data [9], demonstrating the high accuracy of CFD-based numerical models. Consequently, this study uses CFD simulation to predict F_l and F_d, which are a-dimensionalized through the lift (C_l) and drag (C_d) coefficients.

Additionally, [1] highlights that the vehicle's rear is distinctive, with each body style, such as a sedan or hatchback, having unique aerodynamic characteristics that demand a specific geometric solution to optimise airflow. Reference [6] classifies a vehicle as a hatchback if the rear slope is between 0 and 22° and a sedan if the rear is stepped. They affirm that sedans offer significant efficiency, handling, and cost advantages compared to SUVs. They also affirm that sedans are lighter, which enables lower fuel consumption and provides a more agile and comfortable driving experience, especially in urban environments with narrow streets and limited parking. Although SUVs accounted for around 47% of global car sales in 2023 and sedans about 20-21%, sedans still hold a substantial market share in Latin America, about 30-35% in markets like Brazil, where popular models like Toyota Corolla and Nissan Versa rank among the best-sellers [10]. Hence, we chose a sedan for this study.

*CORRESPONDING AUTHOR | Christian V. Rodriguez | ✉ C25183@utp.edu.pe

Reference [11] mentions that sedan vehicles have two separate recirculation regions at the rear window and trunk, unlike hatchbacks with a large recirculation region. Installing a rear wing on the sedan prevents the formation of a recirculation zone above the rear window by generating high pressure with the wing. Reference [4] found that the car's performance with a rear wing was superior, displaying more excellent aerodynamic properties than the vehicle without a rear wing. Notably, the rear wing is one of the most important and commonly used aerodynamic features at the rear of cars [2]. For example, [12] simulated airflow around two car models, a hatchback and a sedan. When they installed a rear wing in both cars, they achieved the most considerable reduction of 36% decrease in the sedan's C_d with an angle of attack (α) of 0°. The most significant C_d reduction for the hatchback was approximately 43% at α = 0°. In contrast, when [13] added a rear wing to sedans, they found a C_d increase from 0.1923 to 0.28307 (47% increase). This increase is primarily due to the rear wing design. The first car has a smoother, more fluid shape, which helps reduce air resistance, while its rear wing has a more angular and robust design. Meanwhile, the second vehicle has a more rectangular shape, creating a nearly right angle between the roof and trunk, and its rear wing has straight edges with a more rectangular appearance. These findings demonstrate that rear wing shape significantly influences the car's aerodynamics, making it necessary to study each type of rear wing added to the vehicle individually.

For optimal rear wing configuration, [2] affirmed that designers must determine the value of α and the rear wing height (b) to achieve maximum performance. For this reason, they evaluated angles between 0 and 20°, with 0.5° increments, in the study of rear wings shaped by NACA 0012, NACA 4412, and NACA 6412 profiles. The chosen α was 8°, as it yielded the highest lift-to-drag ratio, C_l/C_d, for the NACA 6412 rear wing, with $C_l = -0.1$ at a speed of 72 km/h. This study clearly shows that each type of rear wing has a distinct optimal configuration, which provides the best aerodynamic performance. Additionally, they analysed different rear wing height ratios, b/H (b/H relates the rear wing height from the trunk surface to the height from the trunk to the vehicle's roof), precisely 0.17, 0.39, and 0.61. They obtained the best results with b/H = 0.61, where the C_l/C_d ratio was 3.44. Their results demonstrate that rear wing height impacts the vehicle's aerodynamic efficiency, which makes it necessary to analyse b/H ratios and determine the one that enhances aerodynamics when adding a rear wing to a sedan.

Additionally, [3] used α = −7, −4, −1, 2, 5, and 8° for rear wings with NACA 0012, NACA 4412, and S1223 profiles. They obtained the best results for positive α values. They chose α = 6° as it provided the highest C_l/C_d for the S1223 rear wing (C_l between 0 and −0.2) with vehicle speed (U) of 149 km/h and b/H = 0.39. Additionally, [13] simulated a sedan with and without a rear wing for U = 144 km/h, corresponding to a Reynolds number, Re, of 10^5. They obtained C_l and C_d values equal to 0.03957 and 0.19230 in simulations of cars without a rear wing. Meanwhile, the vehicle with a rear wing showed a 510.77% decrease in C_l (from 0.03957 to −0.16254) and a 47.2% increase in C_d (from 0.19230 to 0.28307). Adding a rear wing to the sedan significantly increases downforce, improving driving stability.

The analysed literature indicates that the rear wing's shape and optimal configuration play a significant role in vehicle aerodynamics. Therefore, further investigation into new rear wing configurations is necessary to determine the potential improvements in stability and efficiency for sedans. Consequently, this study aims to define the optimal rear wing configuration to improve a sedan's stability and aerodynamic efficiency through 2D CFD simulations. In these simulations, rear wings generated with NACA 4412, SD7032, E387, NASA SC(2)-0714, and S826 profiles are tested at low vehicle speed (for example, U = 36 km/h), medium (U = 72 and 108 km/h), and high speed (U = 144 km/h). In this context, we first performed a mesh independence study of the domain formed by the car and the rear wing to identify the mesh at which additional refinements no longer influence the results. With the selected mesh, we simulated the aforementioned rear wings and calculated C_l, C_d, and C_l/C_d values to determine the optimal rear wing configuration (using α between 0 and 15°) to enhance the vehicle's aerodynamics. Next, the fluid behaviour around the sedan with and without a rear wing is analysed. Afterwards, we examined the rear wing height ratios (b/H) with the best aerodynamic performance. Finally, the last section presents the conclusions and proposes ideas generated from this study for future research. Apart from the NACA 4412 profile, the profiles used here have not been previously analyzed in rear-wing applications on sedan cars, which contributes to the value of this research.

2. METHODS AND MATERIAL

2.1 Reynolds-Averaged Navier-Stokes Formulation

The Reynolds-Averaged Navier-Stokes (RANS) equations for a steady, incompressible Newtonian fluid flow are presented in [14], representing the conservation of mass and momentum, respectively:

$$\frac{\partial \overline{u}_i}{\partial x_i} = 0 \tag{1}$$

$$\frac{\partial \left(\overline{u}_i \overline{u}_j\right)}{\partial x_j} = -\frac{1}{\rho}\frac{\partial \overline{p}}{\partial x_i} + \frac{\partial}{\partial x_j}\left(\mu \frac{\partial \overline{u}_i}{\partial x_j} - \overline{u_i' u_j'}\right) \tag{2}$$

$\overline{u}_i$ and u_i' represent the mean and fluctuating velocities, respectively. $\bar{p}$ is the average pressure. ρ and μ are the density and kinematic viscosity.

The simulation of cars with rear wings was primarily conducted using the Standard $k-\varepsilon$ [15], the Realizable $k-\varepsilon$ [9, 12, 16] and the SST $k-\omega$ [17] turbulence models. In the past, both the $k-\varepsilon$ and $k-\omega$ turbulence models had various results in the predictions of C_l [4]. For example, [4] simulated a Land Rover Discovery and concluded that the Realizable $k-\varepsilon$ turbulence model produced more accurate results compared to the Standard $k-\omega$ model, showing a variation of 57.79% for the vehicle without a rear wing and 1.29% for the car with a rear wing in terms of C_l. These results lead us to recognize that the Realizable $k-\varepsilon$ model provides better results than other models when simulating cars with rear wings. Consequently, this study uses the Realizable $k-\varepsilon$ turbulence model with Enhanced Wall Treatment, which has shown better numerical results when compared to experimental measurements, as evidenced in the research by [18].

According to Fu et al. [19], the Realizable k-ε model represents a suitable choice when seeking a balance between accuracy and computational efficiency in CFD simulations. Compared to other models, such as the SST k-ω, the Realizable k-ε model stands out for its improved ability to predict flows with complex shear stresses and recirculation regions, common conditions in aerodynamic applications. Furthermore, the Realizable k-ε model is an alternative that correctly predicts the global flow behavior without requiring detailed treatments in the boundary layer of the computational mesh. The steady-state transport equations for the Realizable $k-\varepsilon$ turbulence model [20] for the turbulent kinetic energy (k) and the turbulent dissipation rate (ϵ) are, respectively:

$$\frac{\partial\left(\rho\overline{u}_j k\right)}{\partial x_j}=\frac{\partial}{\partial x_j}\left[\left(\mu+\mu_t\sigma_k\right)\frac{\partial k}{\partial x_j}\right]+P_k-\rho\epsilon-Y_M \tag{3}$$

$$\frac{\partial\left(\rho\overline{u}_j \epsilon\right)}{\partial x_j}=\frac{\partial}{\partial x_j}\left[\left(\mu+\mu_t\sigma_\epsilon\right)\frac{\partial \epsilon}{\partial x_j}\right]+C_{\epsilon 1}\frac{P_b\epsilon}{k}C_{\epsilon 3}-\rho C_{\epsilon 2}\frac{\epsilon^2}{k+\sqrt{\nu\epsilon}} \tag{4}$$

where μ_t is the turbulent viscosity. P_k represents the production of k. In other words, P_k is the generation of k due to buoyancy. Y_M is the contribution of fluctuating dilation to the total dissipation rate. σ_k, σ_ϵ, $C_{\epsilon 1}$ and $C_{\epsilon 2}$ represent the closure coefficients of the turbulence model, incorporated into the *solver Fluent* 24.1.

We used the SIMPLE algorithm to solve the differential equations. The least-squares cell-based method is employed for gradient evaluation, and second-order schemes are applied for pressure, momentum, k and ϵ. 2D simulations require lower computational costs compared to 3D simulations [8], but the latter provide accurate results. Despite this, 2D simulations are used in this study due to computational resource limitations. According to Bambhania et al. [21], aerodynamic drag, represented by Cd, directly influences fuel consumption. Therefore, reducing C_d helps to decrease the air resistance that the vehicle faces when moving, which in turn improves fuel efficiency.

2.2 Geometry, Domain and Boundary Conditions

Figure 1 shows the geometry of the sedan used in this study. As illustrated in Figure 1, simplifying the sedan's original geometry is essential to prevent excessive detail that would considerably increase the computational mesh's element count [22].

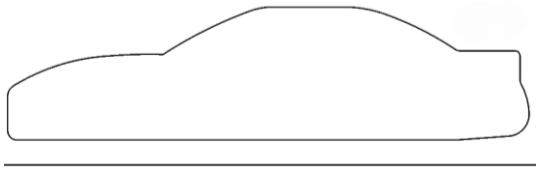

Figure 1. Sedan car geometry model

In previous studies on vehicle simulations, various speeds have been employed, such as 72 km/h [2], 123.12 km/h [17], 140 km/h [1], 144 km/h [1, 12], 150 km/h [5], 180 km/h [18], ranges between 70 km/h and 130 km/h [7], between 96.55 km/h and 128.74 km/h [8], as well as between 144 km/h and 162 km/h [15]. Based on these references, a minimum speed of 36 km/h (equivalent to 10 m/s) was chosen in the present study. This value is lower than those reported in the literature, and it was selected with the aim of exploring aerodynamic behaviour at low speeds, which are relevant in urban contexts or under traffic conditions where vehicles operate with reduced incident airflow. In addition, a maximum speed of 144 km/h (equivalent to 40 m/s), as reported in [1, 12, 15], was adopted to represent high-speed driving conditions. Between these two extremes, two intermediate speeds were selected: 72 km/h and 108 km/h. These values follow a regular sequence of 36, 72, 108, and 144 km/h, allowing the progressive evolution of the vehicle's aerodynamic behaviour to be analysed. The intermediate speeds were strategically chosen since significant differences in flow behaviour are expected to occur at these points.

At the outlet of the domain, a gauge pressure of zero is applied in a similar way as in previous studies [9]. The car and rear wing surfaces are treated as no-slip walls, while the upper and lower boundaries of the domain are considered as symmetry walls [13]. As in [23], a domain height of 2L was used. Regarding the domain length (distance between the inlet and outlet), an intermediate value between those proposed in previous works was selected: 12.17L [15] and 15.8L [23]. A length of 13.25L was chosen for the present study. The computational domain includes two refinement zones (R1 and R2) around the vehicle, as in [14], which allow for a smooth transition in mesh element sizes, from larger elements

in the far-field domain to smaller ones on the surfaces of the car and rear wing. Further details about the domain dimensions and the refinement zones R1 and R2 are presented in Figure 2.

Figure 3 illustrates the geometries of the airfoil profiles used to model the sedan's rear wing. The profiles chosen have shown favourable aerodynamic properties in prior studies [24, 25, 26, 27, 28, 29, 30], which justifies their selection for this research. Here, these profiles are simulated at α from 0 to 15°, with 1° increments. Notably, to the best of the authors' knowledge, the selected profiles (excluding the NACA 4412) have not been previously analyzed for rear-wing applications on sedans.

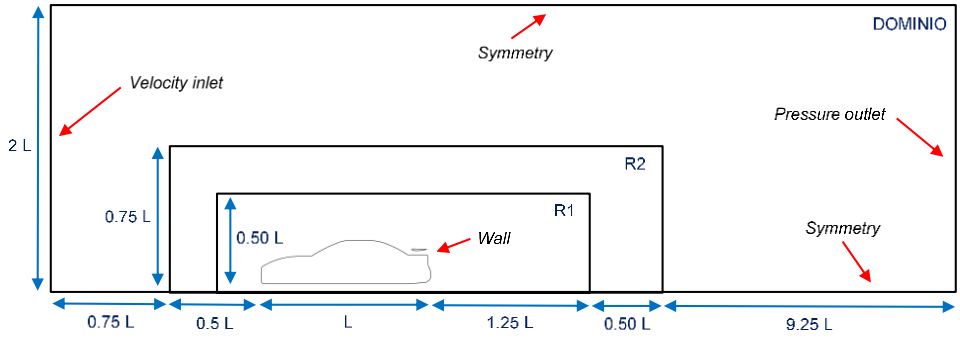

Figure 2. Computational domain

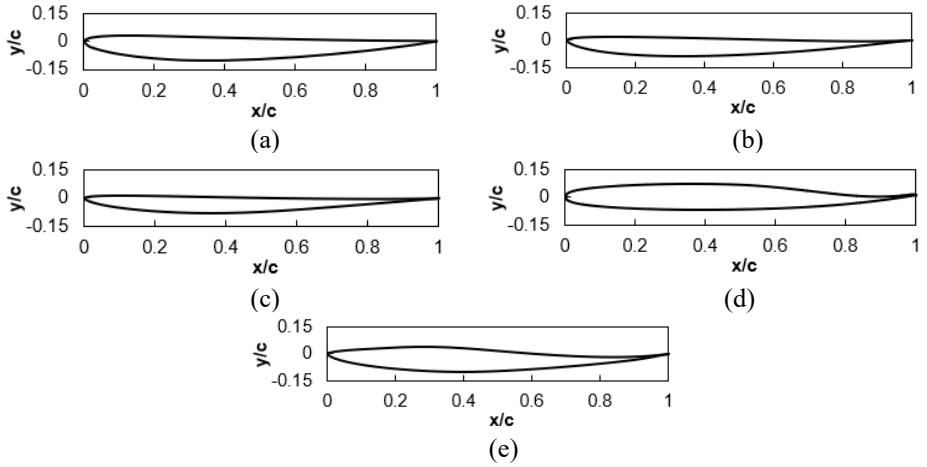

Figure 3. Geometry of the rear wings: (a) NACA 4412, (b) SD7032, (c) E387, (d) NASA SC(2)-0714, and (e) S826 [27]

2.3 Mesh Independence Study

An initial mesh independence study is conducted to determine the characteristics that the mesh used in the rear wing simulations should possess for various U and α. This study analyzes changes in the rear wing's C_l, as the mesh is refined. In this analysis, the sedan's rear wing is modelled using the NACA 4412 airfoil profile, and simulations are conducted for U = 144 km/h and α = 15°. Three mesh configurations are used: Base, Medium, and Fine, with equal element sizes in the far-field domain area. Remarkably, refinements are applied in the regions R1 and R2 and on the surfaces of the car and rear wing. The meshes are composed of triangular elements, a common choice due to their ability to adapt to the curved shapes of the vehicle and rear wing. Details of the element sizes in each region are provided in Table 1. For the configurations used, the Base, Medium, and Fine meshes contain 209 942, 453 840, and 995 968 elements, respectively.

Table 1. Element sizes used in the mesh independence study

Mesh	Domain (m)	R1 (m)	R2 (m)	Car (m)	Rear wing (m)	Elements
Base	0.1	0.050	0.075	0.0050	0.0010	209 942
Medium	0.1	0.020	0.030	0.0020	0.0004	453 840
Fine	0.1	0.011	0.017	0.0011	0.0002	995 968

The boundary layer is essential for achieving accurate results in simulations; therefore, it is crucial to pay special attention to its modelling [4]. The reliability of numerical results related to velocities and pressures near walls is directly affected by the mesh element size in this zone, which must be small enough to capture flow characteristics within the boundary layer. Mesh elements near the surface are known as *inflation*. Previous studies used first cell sizes (y) of $5\text{x}10^{-4}$ m [9] and 10^{-3} m [15]. This study applies 10 boundary layers to the car and rear wing surfaces, with a y of 10^{-5} m and a growth rate of 20% between elements. The dimensionless initial cell sizes (y+) maintain values below 5 for all simulations, as recommended when applying the Realizable k-ε turbulence model with Enhanced Wall Treatment. Based

on the mesh configuration selected from the mesh independence study, an additional validation procedure is conducted using a two-dimensional cylinder, which has been extensively investigated in the literature [31, 32], to validate the numerical model results. Subsequently, multiple simulations of the profiles are performed, and their results are compared from both quantitative and qualitative viewpoints. The validated numerical framework was subsequently applied to the aerodynamic analysis of the rear wings and the sedan vehicle under the same modelling assumptions.

3. RESULTS AND DISCUSSION

3.1 Mesh independence study

Table 2 presents the results of the C_l for the NACA 4412 rear wing, obtained for the different mesh configurations studied. The C_l results from the Medium and Fine meshes are very similar, showing a difference of only 1.52%. Therefore, the Medium mesh is selected for the subsequent simulations, as it is suitable for predicting the aerodynamics of the rear wing without incurring high computational costs.

Table 2. Cl of the NACA 4412 rear wing obtained in the mesh independence study

Mesh	C_l	Error (%)
Base	–0.17338	3.49
Medium	–0.17944	1.52
Fine	–0.18216	

Figure 4 provides details of the Medium mesh. Figure 4(a) shows the size of the elements in the far-field domain, while Figure 4(b) illustrates the refinement zones R1 and R2. The area with the highest refinement is located around the car and rear wing, where greater precision in results is sought and where fluid interaction with the surfaces of the studied objects occurs. The detail of the mesh around the rear wing is illustrated in Figure 4(c), where the highest concentration of mesh elements is found at the leading and trailing edges of the profile due to their curvature. These areas are critical for capturing flow behaviour interacting with the rear wing, especially in predicting flow separation and turbulence. Additionally, the details of the boundary layers on the car and rear wing surfaces are shown in Figure 4(d) and (e), respectively.

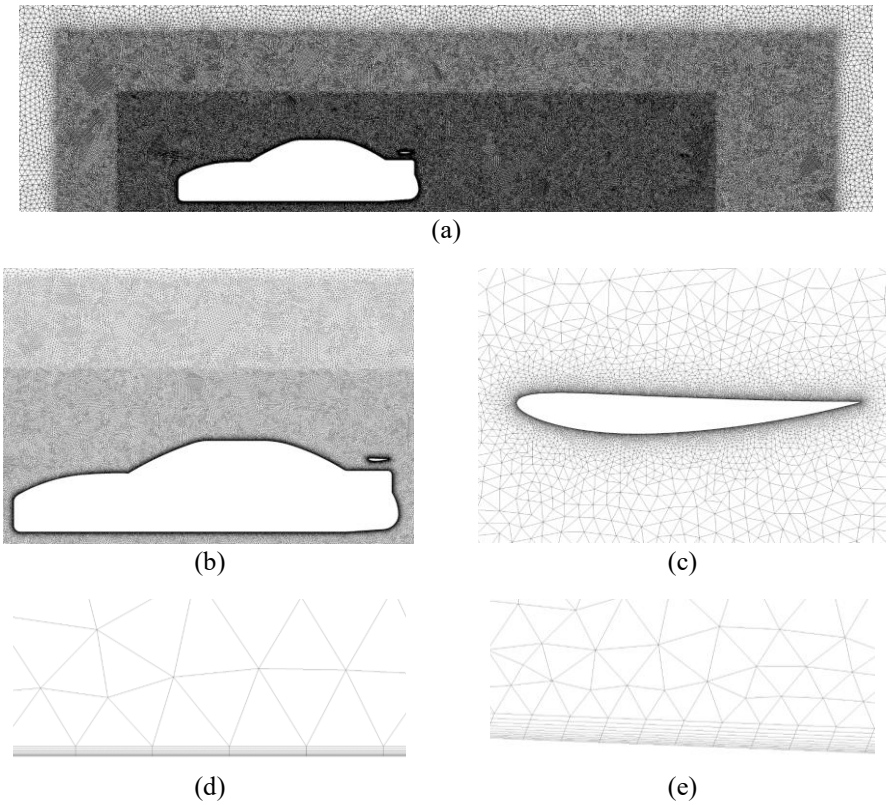

(a) (b) (c) (d) (e)

Figure 4. Details of the Medium mesh: (a) domain, (b) car-rear wing, (c) rear wing, (d) car wall, and (e) rear wing wall

3.2 Validation

In the absence of experimental measurements for the present configuration, a comparative validation of the numerical model was conducted using a benchmark case widely accepted in the literature: the flow around a two-dimensional circular cylinder. This benchmark has been extensively investigated both experimentally and numerically and is commonly employed to assess the reliability of CFD models in aerodynamic applications. We performed the validation

using a two-dimensional cylinder by comparing the experimental data reported in [32] with the numerical results obtained by Rosetti and Fujarra [31], as well as with those of the present study. It is important to note that Rosetti and Fujarra [31] carried out transient flow simulations around the two-dimensional cylinder. In contrast, in this work, we adopted steady-state simulations owing to limitations in the available computational capacity, since transient analyses require a considerably greater numerical effort. Furthermore, we justify the choice of the steady-state approach by the nature of the subsequent analyses conducted on the aerodynamic profiles and the sedan-type vehicle. The mesh generated for the validation is shown in Figure 5.

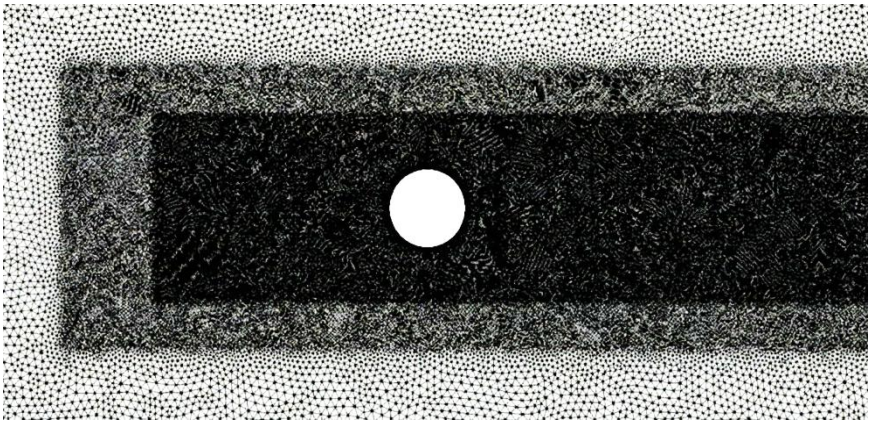

Figure 5. Details of the two-dimensional cylinder mesh

The simulations were carried out considering the cylinder position as specified in [31] and by evaluating different Reynolds number values (R_e = 1,000, 10,000, 100,000, and 500,000). Under these conditions, the drag coefficient (C_d) obtained in the present study exhibited a trend consistent with the experimental data reported in [32] (see Figure 6), although some discrepancies were observed with respect to the results reported in [31]. Overall, the C_d value decreased progressively with increasing R_e. For R_e = 1,000, 10,000, 100,000, and 500,000, C_d values of 1.12859, 0.68240, 0.44681, and 0.59554 were obtained, respectively. This behaviour can be associated with flow regime transition and boundary-layer separation phenomena. The discrepancies between the numerical results obtained in this work and the experimental data can be primarily attributed to the limitations of the turbulence model employed, the type of simulation adopted, and the two-dimensional simplification considered. In particular, steady-state simulations are unable to capture the temporal fluctuations and vortex shedding characteristic of the flow around a cylinder. Nevertheless, despite the simplifications inherent to the steady-state approach, the overall prediction of the flow behaviour was found to be satisfactory.

On the other hand, the differences observed between the C_d values reported in [31] and those obtained in the present study are mainly due to the type of simulation performed, namely transient simulations in [31] and steady-state simulations in this work. It is worth noting that transient simulations allow a more accurate representation of temporal fluctuations and flow dynamics around the cylinder when compared with steady-state simulations. As shown in Figure 6, for R_e = 1,000, the results of the present study are in closer agreement with the experimental data, whereas for R_e = 100,000, a better agreement is observed for the results reported in [31]. This benchmark case was selected because it allows the evaluation of aerodynamic force coefficients under flow conditions that are representative of those analysed in the present study, thereby providing a meaningful basis for assessing the predictive capability and robustness of the numerical approach adopted.

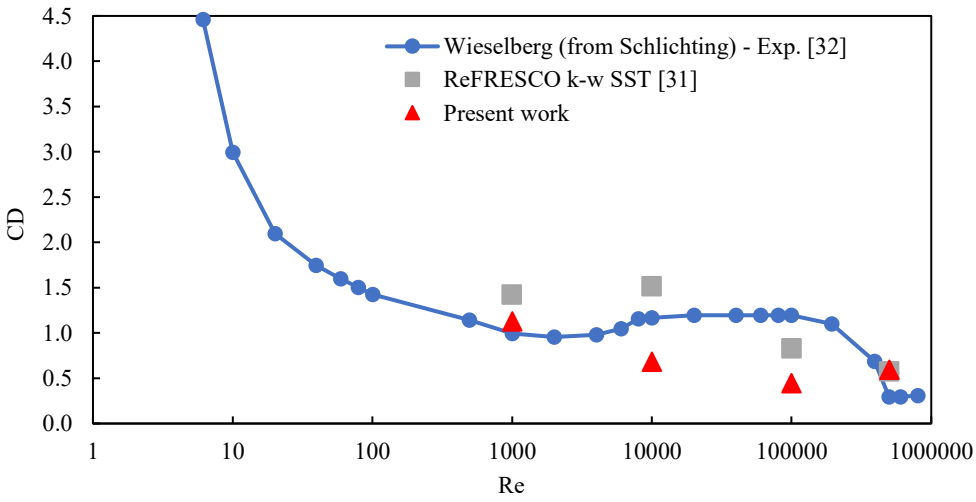

Figure 6. Numerical results of the present work [31], and experimental data [32] from the C_d for different R_e

Overall, despite the inherent limitations associated with steady-state simulations and two-dimensional modelling, the comparative results demonstrate that the numerical model employed in this work is capable of reproducing the main aerodynamic trends of the benchmark case in a physically consistent manner. Consequently, this comparative validation supports the reliability and reproducibility of the numerical methodology applied in the subsequent analysis of the rear wings and the sedan vehicle.

3.3 Optimal Configuration of the Rear Wings

Figure 7 compares the C_l values of the control surfaces made from the NACA 4412, SD7032, E387, NASA SC(2)-0714, and S826 airfoil profiles as a function of α between 0 and 15° and U = 36, 72, 108 and 144 km/h. The optimal airfoil has the lowest drag coefficient C_l, for each speed analyzed, as shown in Figure 7. This airfoil generates the highest negative lift, which is desirable in car rear wings, as it improves stability during vehicle handling. Figure 7(a) illustrates that for U = 36 km/h, the S826 airfoil has the lowest C_l for α from 0 to 4°; however, for α higher than 5°, the NACA 4412 airfoil shows the best C_l. The E387 airfoil, on the other hand, presents relatively high C_l values for almost all α. The SD7032 and NASA SC(2)-0714 airfoils generally show intermediate C_l values, surpassing the other profiles only when α = 7°. The NACA 4412 airfoil shows the best C_l (–0.19358) at α = 9° for U = 36 km/h.

On the other hand, for U = 72 km/h (see Figure 7(b)), it is observed that the S826 airfoil has the lowest C_l at 0°< α < 5°. Moreover, this profile shows good C_l values for 7° < α < 9°, with the best C_l = -0.21445 at α = 7°. The NASA SC(2)-0714 airfoil shows the best C_l for 10° < α < 12°, suggesting that this profile is more effective at relatively high α values. The NACA 4412 airfoil stands out for α > 12°, having the lowest C_l. In contrast, the E387 airfoil presents relatively high C_l values, especially for α higher than 5°. The SD7032 airfoil generally shows intermediate C_l values within the studied α range. Similarly, at a speed of 108 km/h, Figure 7 (c) shows that the S826 airfoil exhibits the lowest C_l in the range of 0° < α < 7°, but for higher α values, the NASA SC(2)-0714 airfoil displays superior C_l values. Furthermore, the best C_l for U = 108 km/h applies for the S826 profile at α = 9° (–0.21883) and α = 7° (–0.21838). The E387 airfoil presents relatively high C_l values at most angles, especially for α higher than 7°. The NACA 4412 and SD7032 airfoils present medium C_l values across the entire α range studied.

Finally, for a speed of 144 km/h (see Figure 7(d)), the S826 airfoil has the lowest C_l for 0° < α < 9°, while for higher α values, the NACA 4412 and NASA SC(2)-0714 profiles show better C_l values. Furthermore, the NASA SC(2)-0714 airfoil shows the best C_l for this speed, with a value of –0.22829 at α = 10°. The E387 airfoil shows the worst C_l values at almost all α values, and the SD7032 airfoil, similar to the other studied speeds, also shows intermediate C_l values. In general, for all speeds, the E387 airfoil shows the worst C_l values for α higher than 5°, while the SD7032 and S826 airfoils present intermediate C_l values for α higher than 8°. Notably, Figure 7 shows that the S826 airfoil presents the best C_l for α higher than 4° (U = 36 and 72 km/h) and for α higher than 9° (U = 108 and 144 km/h). Additionally, the NACA 4412 and NASA SC(2)-0714 profiles show the lowest C_l for α higher than 9°.

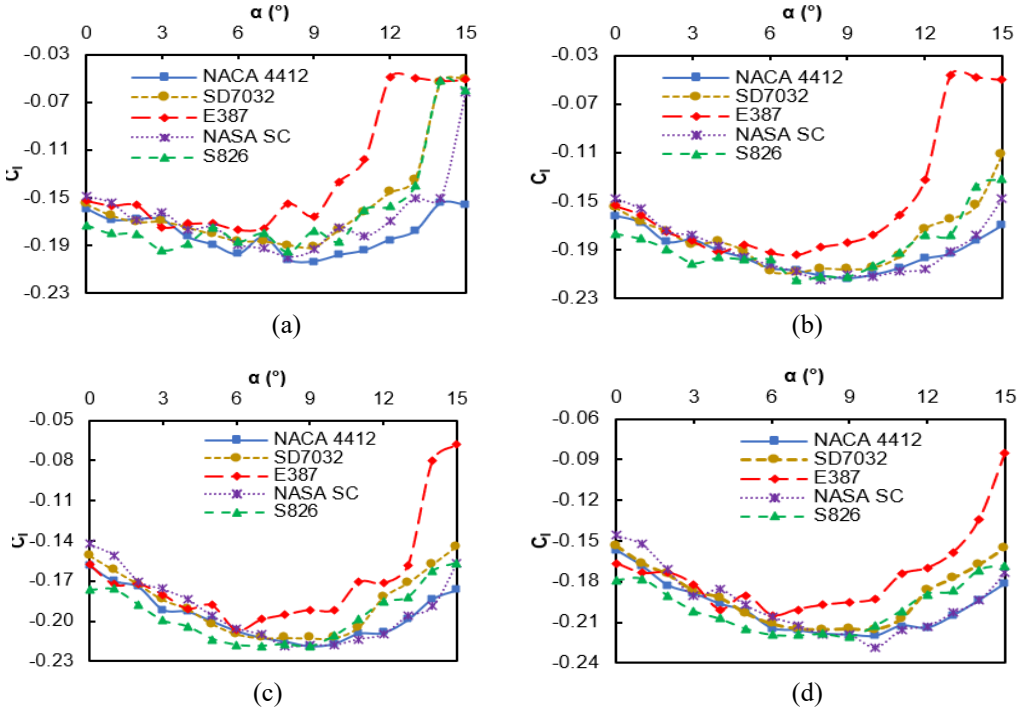

Figure 7. Lift coefficient of the rear wings for speeds of (a) 36 km/h, (b) 72 km/h, (c) 108 km/h, and (d) 144 km/h

The findings presented in this section suggest that, for several driving speeds of the sedan car, various rear wings incorporated into it exhibit the best C_l, with the suitable configurations being the NACA 4412 profile at α = 9° (U = 36 km/h), S826 at α = 7° (U = 72 and 108 km/h), and NASA SC(2)-0714 at α = 10° (U = 144 km/h). Therefore, depending

on the typical driving speed of the sedan car user, the vehicle designer should choose the type of airfoil and angle for the rear wing, or the vehicle must be capable of changing α.

Figure 8 presents the optimal C_l/C_d values for the NACA 4412, SD7032, E387, NASA SC(2)-0714, and S826 rear wings at U = 36 and 72 km/h. The C_l/C_d ratio indicates the aerodynamic efficiency of an airfoil in generating lift relative to the drag it produces. In the context of a vehicle's rear wing, a high C_l/C_d ratio is desirable as it indicates better efficiency in generating aerodynamic load for vehicle stability while minimizing drag. In this regard, as seen in Figure 8(a), the best C_l/C_d ratios belong to the S826 (44.92) and E387 (36.66) profiles, at α = 12° and 10°, respectively, for U = 36 km/h. The SD7032 profile presents intermediate C_l/C_d values. Figure 8(b) shows that the S826 and SD7032 profiles have the best Cl/Cd ratios for U = 108 km/h, with values of 111.47 and 78.46, respectively, at α = 13°. In general, the NACA 4412 and NASA SC(2)-0714 profiles show the lowest C_l/C_d ratios for most of the α values studied at both 36 and 108 km/h. Therefore, the S826 profile is an excellent option for a rear wing (at both low and high speeds) when maximizing aerodynamic load (better stability in driving) while minimizing drag (lower fuel consumption) is required.

It is important to note that the rear-wing's optimal configuration will depend on its adhesion's main objective, that is, whether you are looking to improve driving stability (lower C_l), the vehicle designer should select the NACA 4412 (U = 36 km/h, α = 9°), S826 (U = 72 and 108 km/h, α = 7°), or NASA SC(2)-0714 (U = 144 km/h, α = 10°) profiles accordingly. On the other hand, if the objective is to achieve a balance between enhanced stability (lower C_l) and reduced drag (lower C_d), the S826 profile is a good selection at α = 12° (low driving speeds, U = 36 km/h) or α = 13° (high speeds, U = 108 km/h).

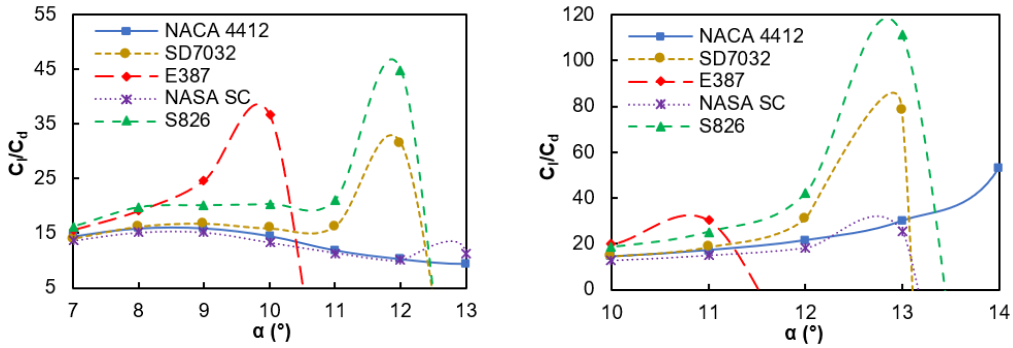

Figure 8. Cl/Cd of the rear wing for speeds of (a) 36 km/h and (b) 72 km/h

Additionally, the flow behaviour around the NACA 4412 (α = 9°), S826 (α = 7°), and NASA SC(2)-0714 (α = 10°) rear wings for U = 36, 72, 108, and 144 km/h is analyzed qualitatively (with more details in Figure 9). Furthermore, the α values chosen for each rear wing correspond to those that generate the lowest C_l (see Figure 7). Figure 9 illustrates the velocity contours around each rear wing, with a colour scale ranging from red (indicating higher velocities) to blue (indicating lower velocities). As expected, the stagnation point (zero velocity) is located on the upper surface of the rear wing. In contrast, the area of highest velocity is found on the lower surface, where the air accelerates as it passes over the curved surface. For all profiles, the flow velocities over the upper surface are lower (higher pressures) compared to those on the lower surface (lower pressures), which generates a downward force (negative lift).

In Figure 9(a) to (c) for U = 36 km/h, the NACA 4412 rear wing shows a larger area with relatively high velocities (green colour) beneath its lower surface (lower pressures), compared to the other rear wings, which causes it to have the lowest C_l (–0.20334). Figure 9 (d) to (f) for 72 km/h and Figure 9 (g) to (i) for 108 km/h show that the S826 rear wing has the largest area with high velocities (beneath its lower surface), which is why it shows the best C_l values for U = 72 km/h (–0.21445) and 108 km/h (–0.21883). Finally, in Figure 9 (j) to (l), it can be seen that the NASA SC(2)-0714 rear wing generates the highest fluid velocity beneath its lower surface, which results in the lowest C_l of –0.22829 for U = 144 km/h. The results suggest that the maximum velocity or a larger area of high velocities (low pressures) directly influence the C_l generation of the rear wings studied in this work. These results can be explained using Bernoulli's principle, which states that as a fluid's velocity increases, its pressure decreases, accounting for lift generation. When rear wings are installed on the vehicle, the regions of positive pressure on the upper surface grow, enhancing the car's C_l.

Based on the simulation results, the velocities on the upper side of the rear wing are lower than those on the lower side. This velocity difference results in higher pressure on the rear wing's upper surface than on the lower surface, thereby increasing the negative lift. A low-pressure region forms as the flow accelerates underneath the rear wing, amplifying the downward force exerted on the vehicle.

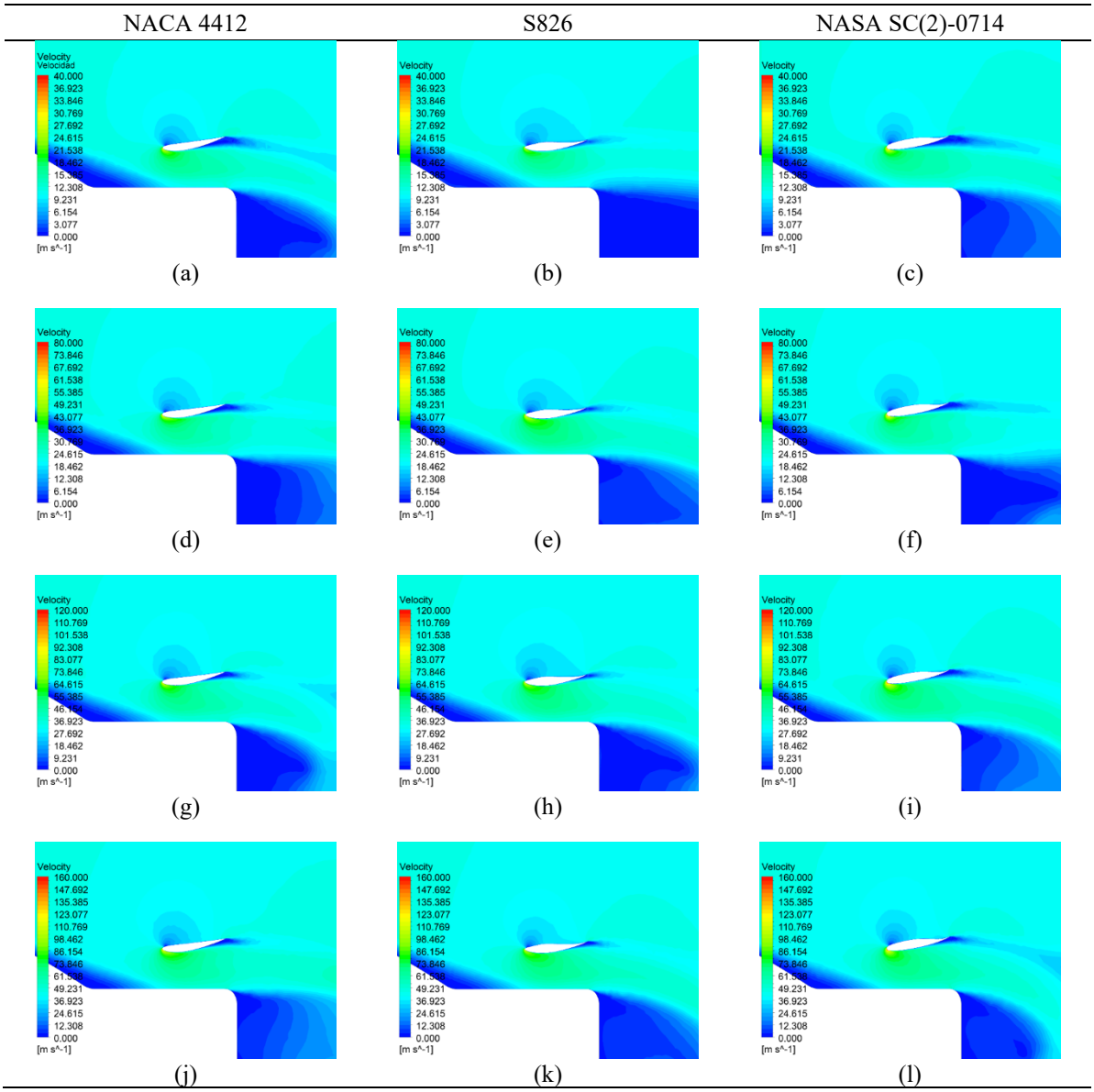

Figure 9. Flow distribution around the NACA 4412, S826, and NASA SC(2)-0714 rear wings for velocities of (a-c) 36 km/h, (d-f) 72 km/h, (g-i) 108 km/h, and (j-l) 144 km/h

3.4 Study of the Car with and without the Rear Wing

Figure 10 shows the flow distribution around the vehicle in two configurations (without rear wing and with rear wing) for U = 36, 72, 108, and 144 km/h. The rear wings are simulated with their configuration of lowest C_l, that is, NACA 4412 with α = 9°, S826 with α = 7°, and NASA SC(2)-0714 with α = 10°. Generally, the airflow pattern in front of the vehicle is similar in both configurations. However, significant differences are observed at the rear due to the presence or absence of the rear wing. The recirculation zone over the trunk is larger when there is no rear wing, as seen in Figure 10(a) to (d). Additionally, as the vehicle speed increases, the turbulent zone at the rear, represented by very low velocities (blue colour), also increases. The C_d values for the vehicle without a rear wing are 0.14371, 0.14349, 0.14363, and 0.14391 for U = 36, 72, 108, and 144 km/h, respectively. Furthermore, these values show a less than 0.2% variation between them. As for the C_l of the car without a rear wing, values were found for the mentioned speeds of –0.43516, –0.48028, –0.51191, and –0.54918, with an average decrease of 8% as U increases.

Figure 10(e) to (h) show the flow distribution around the car with a rear wing. Furthermore, there is a larger flow separation zone behind the vehicle with a rear wing (blue colour), indicating a larger turbulent zone. This larger zone, compared to the car configuration without a rear wing, generates a higher C_d on the car, with values of 0.21669 (generated by the NACA 4412 rear wing), 0.21201 (S826), 0.23396 (S826), and 0.23336 (NASA SC(2)-0714) for U = 36, 72, 108, and 144 km/h, respectively. This indicates that the rear wings added to the car cause its C_d to increase by 50.79%, 47.75%, 62.89% and 62.16% for U = 36, 72, 108, and 144 km/h, respectively. On the other hand, there is an improvement in the C_l, decreasing its value by 202.34%, 208.14%, 245.93% and 220.29% for the same speeds mentioned. The findings demonstrate that the rear wing improves the vehicle's stability during driving (lower C_l) but generates higher aerodynamic drag (higher C_d), which increases fuel consumption. Despite this, improving the vehicle's stability, which translates into

better safety and control during driving, may justify the increased fuel consumption, making prioritizing stability the preferred decision in many cases [13].

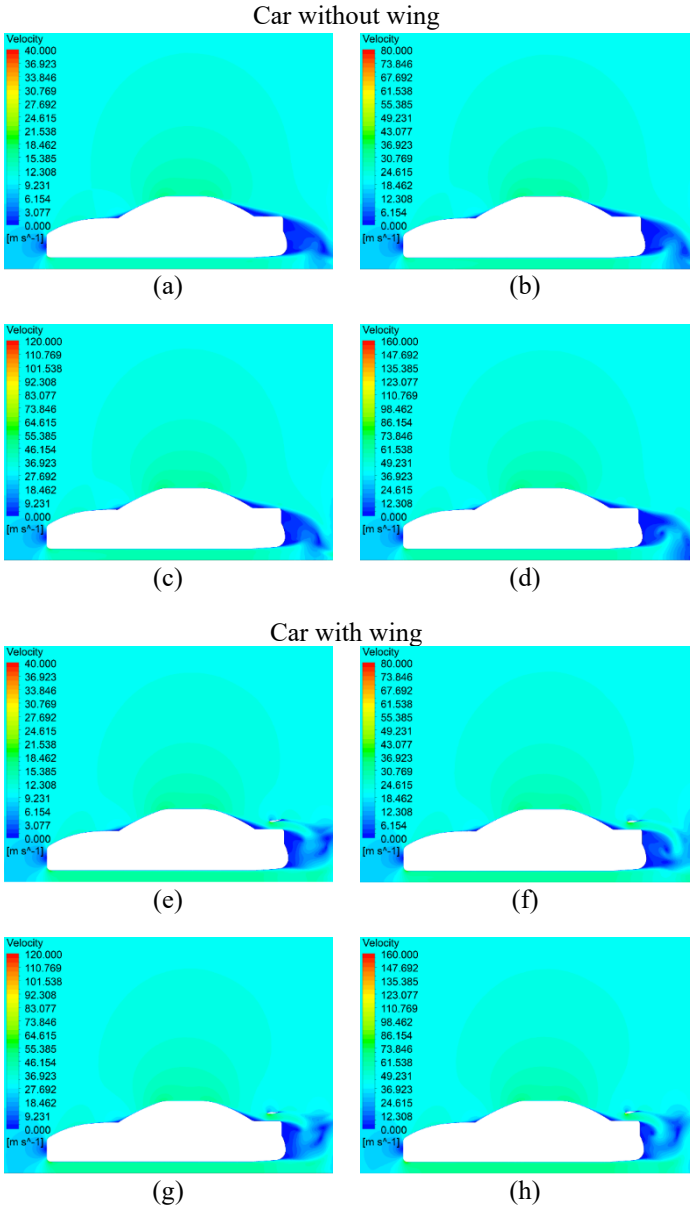

Figure 10. Flow distribution around the car without a wing for (a) U = 36 km/h, (b) U = 72 km/h, (c) U = 108 km/h, and (d) U = 144 km/h; and around the car with a wing for (e) U = 36 km/h (NACA 4412), (f and g) U = 72 and 108 km/h (S826), and (h) U = 144 km/h (NASA SC(2)-0714)

3.5 Flow analysis for Different Rear Wing Heights

This section analyzes the flow around the sedan for various b/H. b refers to the height from the trunk surface to the rear wing, while H represents the height from the trunk to the vehicle's roof (see Figure 11). Figure 12 presents the results of the airflow simulations around the sedan with a rear wing. The rear wing has three height ratios (b/H = 0.17, 0.39, and 0.61). The profiles used in these simulations correspond to the NACA 4412 (α = 9°, U = 36 km/h), S826 (α = 7°, U = 72 and 108 km/h), and NASA SC(2)-0714 (α = 10°, U = 144 km/h). From a qualitative standpoint, the wake formed behind the car and rear wing (blue colour) corresponds to low velocities and high turbulence, contributing to increased drag generation.

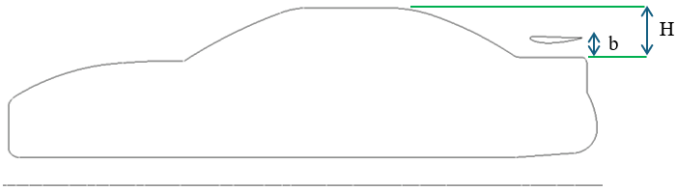

Figure 11. b and H heights of the sedan vehicle

Regarding U = 36 km/h (see Figure 12(a) to (c)), the C_l obtained with the NACA 4412 rear wing (car and rear wing) is -0.78585 for the lower height ratio (b/H = 0.17), while for a higher height ratio, the C_l decreases to −1.31568 (b/H = 0.39). For the highest b/H ratio of 0.61, the C_l is −0.92140. Concerning C_d, its lowest value of 0.16429 is calculated at b/H = 0.17, followed by values of 0.17209 and 0.21669 for the b/H ratios of 0.61 and 0.39, respectively. These findings suggest that if the goal is to maximize vehicle stability, vehicle designers should select the b/H = 0.39 rear wing height ratio, as it provides the lowest C_l, although it significantly increases the C_d. On the other hand, the b/H = 0.61 configuration offers a balance between C_l and C_d.

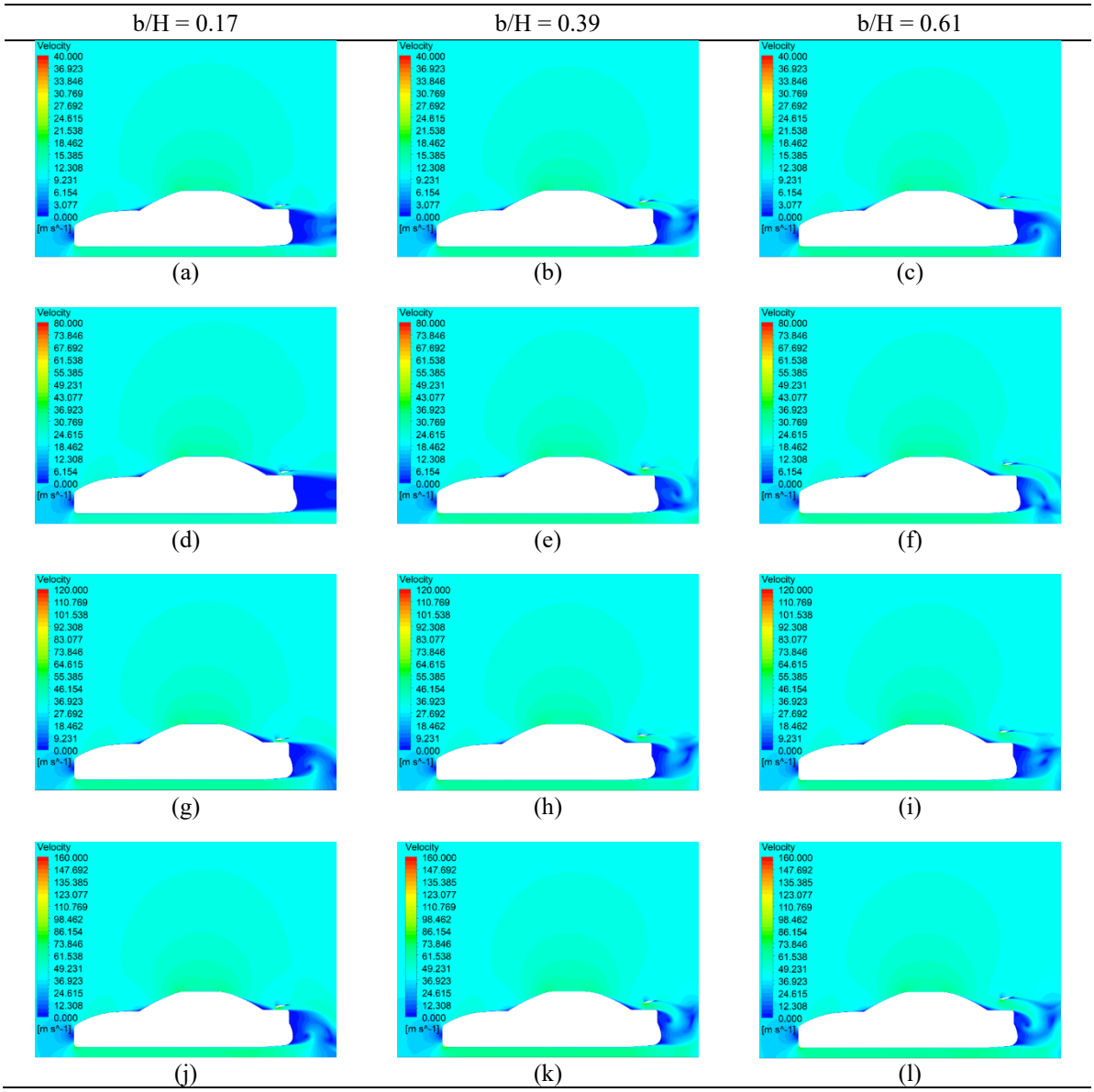

Figure 12. Flow distribution around the car at different wing heights for (a-c) U = 36 km/h (NACA 4412), (d-f) U = 72 km/h (S826), (g-i) U = 108 km/h (S826), and (j-l) U = 144 km/h (NASA SC(2)-0714)

The C_l values of S826 airfoil wing achieved for the b/H ratios of 0.17, 0.39, and 0.61 are −0.56724, −1.47995, and −0.98939, respectively, for U = 72 km/h. Figure 12 (d) to (f) further detail the fluid behaviour. Similarly, the C_d values calculated for the mentioned heights are 0.12134, 0.21201, and 0.17358, respectively. As with the NACA 4412 rear wing, the S826 rear wing shows the lowest C_l at b/H = 0.39, while the lowest C_d is generated when b/H = 0.17. Notably, for U = 108 km/h, the S826 rear wing provides the lowest Cl (−1.77083) at b/H = 0.39, and the lowest Cd (0.16389) at b/H = 0.61 (see Figure 12(g) - (i)). For U = 144 km/h (Figure 12 (j) to (l)), the C_l values generated by the NASA SC(2)-0714 rear wing are −1.12896, −1.75895, and −1.17070 for the b/H ratios of 0.17, 0.39, and 0.61, respectively. Meanwhile, for the mentioned heights, the C_d values are 0.18070, 0.23336, and 0.18165, respectively. Similar to the other rear wings mentioned, the b/H = 0.39 provides the best C_l, and the b/H = 0.17 generates a balance between C_l and C_d.

4. CONCLUSIONS

In the present study, we determined the optimal configuration of a rear wing installed on the trunk of a sedan by comparing the C_l and C_d, as well as the C_l/C_d ratio of different rear wings shaped from the NACA 4412, SD7032, E387,

NASA SC(2)-0714, and S826 profiles. Good aerodynamics are crucial for reducing both lift (positive) and drag, thereby improving aerodynamic efficiency and driving stability. Next, we conducted a mesh independence study for the numerical model of the sedan and rear wing. The results indicated that the Medium mesh is ideal for the other simulations, as it effectively predicts the aerodynamics of the rear wing without incurring high computational costs. Notably, the calculated error between the Medium and Fine meshes was only 1.52%. Afterwards, we defined the C_l, C_d, and C_l/C_d ratios for different α values of the rear wings. Using the Medium mesh, we performed simulations for the rear wings in various configurations with α ranging from 0° to 15° and U = 36, 72, 108, and 144 km/h. When comparing the C_l/C_d ratios of the rear wings, we found that the S826 rear wing was the most efficient from an aerodynamic standpoint, as it showed the best results at both low (C_l/C_d = 44.92, U = 36 km/h) and high speeds (C_l/C_d = 111.47, U = 108 km/h), making it ideal for maximizing aerodynamic load with minimal drag. It is worth noting that the E387 rear wing excelled at low speeds, while the SD7032 performed well at high speeds. In contrast, the NACA 4412 and NASA SC(2)-0714 rear wings showed the worst Cl/Cd ratios. In this regard, the selection of the rear wing will depend on the desired balance between stability (lower C_l) and drag (lower C_d).

Additionally, we identified the optimal rear-wing angle at different vehicle speeds. The analysis revealed that at 36 km/h, the NACA 4412 rear wing was most effective at α = 9°, with a C_l of -0.20334. At 72 km/h, the S826 rear wing generated negative lift at α = 7°, with a C_l of –0.21445. At 108 km/h, the S826 remained the best, with a C_l of –0.21883, maintaining the same α. Finally, at 144 km/h, the NASA SC(2)-0714 rear wing excelled with α = 10° and a C_l of -0.22829. The airflow behaviour around the car, both with and without the rear wing, was also analyzed. In the qualitative airflow analysis, the airflow behind the car was less turbulent without the rear wing, resulting in a lower C_d of 0.14369. The use of the NACA 4412 (U = 36 km/h, α = 9°, C_d = 0.21669), S826 (U = 72 and 108 km/h, α = 7°, C_d = 0.21201 and 0.23396), and NASA SC(2)-0714 (U = 144 km/h, α = 10°, C_d = 0.23336) rear wings increased the turbulence, and consequently the C_d, reflecting higher drag and energy consumption of the vehicle. Despite this, the rear wings improved the vehicle's stability by significantly reducing the C_l at all speeds studied.

Finally, despite the increase in drag, the rear wings improved the vehicle's stability by significantly reducing the lift coefficient (C_l) under all driving conditions studied. In this context, the following profiles were employed: NACA 4412 with α = 9° at 36 km/h, S826 with α = 7° at 72 and 108 km/h, and NASA SC(2)-0714 with α = 10° at 144 km/h. Based on these configurations, the optimal rear wing height was determined by evaluating b/H ratios of 0.17, 0.39, and 0.61. The results showed that, in general, as the b/H ratio increases, the C_l improves, but the C_d also increases. The configuration with b/H = 0.39 yielded the highest aerodynamic load (lowest C_l), while b/H = 0.17 produced the lowest drag coefficient. Lastly, the b/H = 0.61 ratio represented a compromise between improved stability (lower C_l) and energy efficiency (lower C_d). Although this study provides valuable insights into the aerodynamic performance of rear wings on sedan-type vehicles, it is important to acknowledge the limitations stemming from the use of idealised simulation conditions. For future work, it is recommended to expand the analysis by incorporating real-world driving factors, such as crosswinds, yaw angles, and unsteady flow conditions. Moreover, transient and 3D simulations should be conducted to evaluate the aerodynamic behaviour under more realistic operating conditions, including vehicle motion, variable turbulence intensities, and road-induced disturbances. These enhancements will not only improve the physical fidelity of the simulations but also support the design of rear wings that are robust under actual driving environments. Complementary wind tunnel or on-road testing is also encouraged to further validate the numerical findings and bridge the gap between simulation and practice.

ACKNOWLEDGEMENTS

This research was not funded by any grants from public, private, or nonprofit funding agencies. To the Vice-Rectorate for Research of the Universidad Nacional de Ingeniería, Lima, Peru

CONFLICT OF INTEREST

The authors declare that they have no conflicts of interest.

AUTHORS CONTRIBUTION

Juan A. Guevara (Methodology; Formal Analysis; Software; Writing – Initial Draft)

Christian V. Rodriguez (Conceptualization; Supervision; Writing – Review and Editing)

Dennys D. De La Torre (Supervision; Writing - Review & Editing)

REFERENCES

[1] M. Fabian, R. Huňady, and O. Lagos, "Design modification of the combi-type body considering the impact on vehicle aerodynamics - Case study," *Manufacturing Technology*, vol. 23, no. 6, pp. 801–809, 2023.

[2] H. Kumar, A. Pingua, and S. Gupta, "Effect of different wing profile and wing height on aerodynamic performance of a sedan vehicle," in *International Conference on Mechanical and Production Engineering*, 2019, pp. 30–34.

[3] H. Eftekhari, A. S. M. Al-Obaidi, and S. Eftekhari, "The effect of spoiler shape and setting angle on racing cars aerodynamic performance," *Indonesian Journal of Science and Technology*, vol. 5, no. 1, pp. 11–20, 2020.

[4] M. H. Roslan, H. Hasbullah, T. Ramesh, D. Hissein Didane, B. Manshoor, and H. A. Kabrein, "Effect of a spoiler on the aerodynamic performance of a race car on track using two different turbulence models," *Journal of Design for Sustainable and Environment*, vol. 5, no. 2, pp. 28–37, 2023.

[5] D. S. Nath, P. C. Pujari, A. Jain, and V. Rastogi, "Drag reduction by application of aerodynamic devices in a race car," *Advances in Aerodynamics*, vol. 3, no. 1, p. 4, 2021.

[6] G. Sivaraj, K. M. Parammasivam, and G. Suganya, "Reduction of aerodynamic drag force for reducing fuel consumption in road vehicle using basebleed," *Journal of Applied Fluid Mechanics*, vol. 11, no. 6, pp. 1489–1495, 2018.

[7] R. C. Das and M. Riyad, "CFD analysis of passenger vehicleat various angle of rear end spoiler," *Procedia Engineering*, vol. 194, pp. 160–165, 2017.

[8] T. P. O'Driscoll and A. R. Barron, "CFD analysis of the location of a rear wing on an Aston Martin DB7 in order to optimize aerodynamics for motorsports," *Vehicles*, vol. 4, no. 2, pp. 608–620, 2022.

[9] S.-Y. Cheng and S. Mansor, "Influence of rear-roof spoiler on the aerodynamic performance of hatchback vehicle," *MATEC web of conferences*, vol. 90, p. 01027, 2017.

[10] Statista, "Global car sales distribution by type 2023." Accessed: Dec. 01, 2023. [Online]. Available: https://www.statista.com/statistics/276567/global-market-share-of-passenger-car-sales-by-vehicle-type/

[11] R. D. R. Mariaprakasam, S. Mat, P. M. Samin, N. Othman, M. Ab Wahid, and M. Said, "Review on flow controls for vehicles aerodynamic drag reduction," *Journal of Advanced Research in Fluid Mechanics and Thermal Sciences*, vol. 101, no. 1, pp. 11–36, 2023.

[12] R. Bahoosh, M. Rohani, and M. R. Saffarian, "Numerical simulations of spoiler's effect on a hatchback and a sedan car exposed to crosswind effect," *Journal of Applied and Computational Mechanics*, vol. 9, no. 2, pp. 346–356, 2023.

[13] M. Z. Nawam, M. A. M. Rosli, and N. A. S. Rosli, "Simulation study on the effect of rear-wing spoiler on the open aerodynamic performance of sedan vehicle," *Journal of Advanced Research in Fluid Mechanics and Thermal Sciences*, vol. 49, no. 2, pp. 146–154, 2018.

[14] M. Abid, H. A. Wajid, M. Z. Iqbal, S. Najam, A. Arshad, and A. Ahmad, "Design and analysis of an aerodynamic downforce package for a formula student race car," *IIUM Engineering Journal*, vol. 18, no. 2, pp. 212–224, 2017.

[15] J. Broniszewski and J. Piechna, "A fully coupled analysis of unsteady aerodynamics impact on vehicle dynamics during braking," *Engineering Applications of Computational Fluid Mechanics*, vol. 13, no. 1, pp. 623–641, 2019.

[16] A. Al Saadi and A. Hassanpour, "Simulations of aerodynamic behaviour of a super utility vehicle using computational fluid dynamics," *Advances in Automobile Engineering*, vol. 5, no. 1, pp. 1–5, 2016.

[17] J. Dušek, M. Chrust, and G. Bouchet, "Transitional Dynamics of Freely Falling Discs," in *Notes on Numerical Fluid Mechanics and Multidisciplinary Design*, vol. 133, 2016, pp. 105–116.

[18] C.-H. Tsai, L.-M. Fu, C.-H. Tai, Y.-L. Huang, and J.-C. Leong, "Computational aero-acoustic analysis of a passenger car with a rear spoiler," *Applied Mathematical Modelling*, vol. 33, no. 9, pp. 3661–3673, 2009.

[19] C. Fu, M. Uddin, and A. C. Robinson, "Turbulence modeling effects on the CFD predictions of flow over a NASCAR Gen 6 racecar," *Journal of Wind Engineering and Industrial Aerodynamics*, vol. 176, pp. 98–111, 2018.

[20] M. Dickison, M. Ghaleeh, S. Milady, S. Subbakrishna, L. T. Wen, and M. Al. Qubeissi, "Investigation into the aerodynamic performance of a concept sports car," *Journal of Applied Fluid Mechanics*, vol. 13, no. 2, pp. 583–601, 2020.

[21] M. P. Bambhania and J. Deepak, "Numerical simulation of two-dimensional ahmed body numerical simulation of two-dimensional ahmed body abstract," *International Journal of Fluid and Thermal Engineering*, vol. 1, pp. 21-26, 2016.

[22] K. Koca, M. S. Genç, H. H. Açıkel, M. Çağdaş, and T. M. Bodur, "Identification of flow phenomena over NACA 4412 wind turbine airfoil at low Reynolds numbers and role of laminar separation bubble on flow evolution," *Energy*, vol. 144, pp. 750–764, 2018.

[23] A. Buljac, I. Džijan, I. Korade, S. Krizmanić, and H. Kozmar, "Automobile aerodynamics influenced by airfoil-shaped rear wing," *International Journal of Automotive Technology*, vol. 17, no. 3, pp. 377–385, 2016.

[24] J.-H. Xu, W.-P. Song, Z.-H. Han, and Z.-H. Zhao, "Effect of mach number on high-subsonic and low-Reynolds-number flows around airfoils," *International Journal of Modern Physics B*, vol. 34, no. 14n16, p. 2040112, 2020.

[25] A. B. M. T. Hasan and M. M. Alam, "RANS computation of transonic buffet over a supercritical airfoil," *Procedia Engineering*, vol. 56, pp. 303–309, 2013.

[26] J. Bartl, K. F. Sagmo, T. Bracchi, and L. Sætran, "Performance of the NREL S826 airfoil at low to moderate Reynolds numbers—A reference experiment for CFD models," *European Journal of Mechanics-B/Fluids*, vol. 75, pp. 180–192, 2019.

[27] Airfoil Tools, "Airfoil Database." Accessed: Dec. 30, 2023. [Online]. Available: http://www.airfoiltools.com/

[28] A. Kozelkov, N. Galanov, and A. Kurkin, "Numerical investigation of NASA SC (2)-0714 airfoil icing in a supersonic flow," *Fluids*, vol. 10, no. 10, p. 260, 2025.

[29] F. Mallor, R. Vinuesa, R. Örlü, and P. Schlatter, "High-fidelity simulations of the flow around a NACA 4412 wing section at high angles of attack," *International Journal of Heat and Fluid Flow*, vol. 110, p. 109590, 2024.

[30] F. Mallor, C. Sanmiguel Vila, M. Hajipour, R. Vinuesa, P. Schlatter, and R. Örlü, "Experimental characterization of turbulent boundary layers around a NACA 4412 wing profile," *Experimental Thermal and Fluid Science*, vol. 160, p. 111327, 2025.

[31] G. F. Rosetti, G. Vaz, and A. L. C. Fujarra, "URANS calculations for smooth circular cylinder flow in a wide range of Reynolds numbers: Solution verification and validation," *Journal of Fluids Engineering*, vol. 134, no. 12, 2012.

[32] H. Schlichting and K. Gersten, *Boundary-Layer Theory*. Berlin, Heidelberg: Springer Berlin Heidelberg, 2000.